Optical Review (2018) 25:464–472
https://doi.org/10.1007/s10043-018-0434-3

SPECIAL SECTION: REGULAR PAPER

Optics Awards 2017 (OA 2017)

Optofluidic time-stretch microscopy: recent advances

Cheng Lei[1] · Nao Nitta[2] · Yasuyuki Ozeki[3] · Keisuke Goda[1,2,4]

Received: 29 March 2018 / Accepted: 3 April 2018 / Published online: 11 April 2018

Abstract
Flow cytometry is an indispensable method for valuable applications in numerous fields such as immunology, pathology, pharmacology, molecular biology, and marine biology. Optofluidic time-stretch microscopy is superior to conventional flow cytometry methods for its capability to acquire high-quality images of single cells at a high-throughput exceeding 10,000 cells per second. This makes it possible to extract copious information from cellular images for accurate cell detection and analysis with the assistance of machine learning. Optofluidic time-stretch microscopy has proven its effectivity in various applications, including microalga-based biofuel production, evaluation of thrombotic disorders, as well as drug screening and discovery. In this review, we discuss the principles and recent advances of optofluidic time-stretch microscopy.

Keywords Optofluidic time-stretch microscopy · Machine learning · Microfluidics · High-throughput cell analysis · Single-cell analysis

1 Introduction

Flow cytometry is an indispensable method for valuable applications in numerous fields such as immunology, pathology, pharmacology, molecular biology, and marine biology [1]. There exists a variety of methods to implement flow cytometry. While approaches such as high-throughput analysis [2] and fluorescence-activated cell sorting [3] are feasible for their high throughput and chemical specificity, they remain majorly limited by their necessity for chemical labeling and insensitivity to phenotypic characteristics. In contrast, high-content analysis [4] and imaging flow cytometry [5] can acquire multidimensional cellular information and are thus superior in terms of high accuracy and specificity. However, their throughput is fundamentally limited by the performance of currently available imaging techniques, specifically the frame rate of commercial CCD or CMOS image sensors, which hinders their application to analysis of a large population of cells.

Optofluidic time-stretch microscopy is a newly emerging method addressing the limited throughput by combining the advantages of flow cytometry and imaging. Hence, it provides superior performance in single-cell analysis compared to conventional methods. This enhancement is made possible by combining an optical time-stretch microscope, which images the cells continuously at a high frame rate and a high shutter speed [6, 7], and a microfluidic device, which channels and orders the cells at a high throughput [1, 8]. Specifically, optofluidic time-stretch microscopy is capable of acquiring bright-field images of single cells with a high spatial resolution of 780 nm and an extremely high throughput of 10,000 cells per second [9], corresponding to the image resolution found in conventional imaging-based methods. Owing to the high quality of the cellular images, thousands of morphological features can be extracted from each cellular image, which can be effectively utilized in high-precision and high-accuracy cell detection and analysis in a label-free manner with the assistance of machine-learning methods. Due to its excellent performance in single-cell analysis, optofluidic time-stretch microscopy has been widely applied in various fields to measure different types of

✉ Cheng Lei
leicheng@chem.s.u-tokyo.ac.jp

1 Department of Chemistry, University of Tokyo, Tokyo 113-0033, Japan

2 Japan Science and Technology Agency, Kawaguchi 332-0012, Japan

3 Department of Electrical Engineering and Information Systems, University of Tokyo, Tokyo 113-8656, Japan

4 Department of Electrical Engineering, University of California, Los Angeles, CA 90095, USA

cells, including microalga-based biofuel production [10, 11], evaluation of thrombotic disorders [12], and drug screening and discovery [13].

In this review, we discuss the principles and recent advances of optofluidic time-stretch microscopy. Specifically, in Sect. 2, we introduce the principles of optofluidic time-stretch microscopy, namely its schematic and basic performance. In Sect. 3, we show a few applications of optofluidic time-stretch microscopy, including characterization of microalgal cells for green energy production, detection of aggregated platelets for evaluation of thrombotic disorders, and detection of cellular drug responses for drug screening and discovery. In Sect. 4, we summarize this paper. We hope that this review paper can be useful to researchers who are interested in using this method for their research and development.

2 Principles and basic performance of optofluidic time-stretch microscopy

A typical configuration of optofluidic time-stretch microscopy is schematically shown in Fig. 1. An optofluidic time-stretch microscope consists of three main parts: (i) an optical time-stretch microscope for the imaging of cells at ultrahigh speed, (ii) a microfluidic device for focusing of cells at a high flow rate, and (iii) a digital signal processor for large-scale single-cell analysis based on recorded cellular images. In this section, we discuss the basics of optofluidic time-stretch microscopy, including its principles, typical configuration, and basic performance.

2.1 Schematic of optofluidic time-stretch microscopy

As shown in Fig. 1, an optofluidic time-stretch microscope is composed of several key components: a broadband pulse laser, a temporal disperser, a spatial disperser, a pair of objective lenses, a microfluidic device, a single-pixel photodetector, a digitizer, and a digital signal processor. First, the optical pulses from the broadband pulsed laser are led to the temporal disperser (the fiber spool in Fig. 1), which stretches each pulse in the time domain according to the frequency-dependent differences in transmission velocity in the dispersive element. After that, the pulse is spatially dispersed by the diffraction grating. As a result, different frequency components of the pulse are diffracted at different angles, resulting in a rainbow-like 1D pulse profile. This 1D rainbow pulse is then focused onto the target by the objective lens. Hence, different coordinates on the target are illuminated by the different frequency components of the pulse. In other words, the spatial information of the target is encoded in the

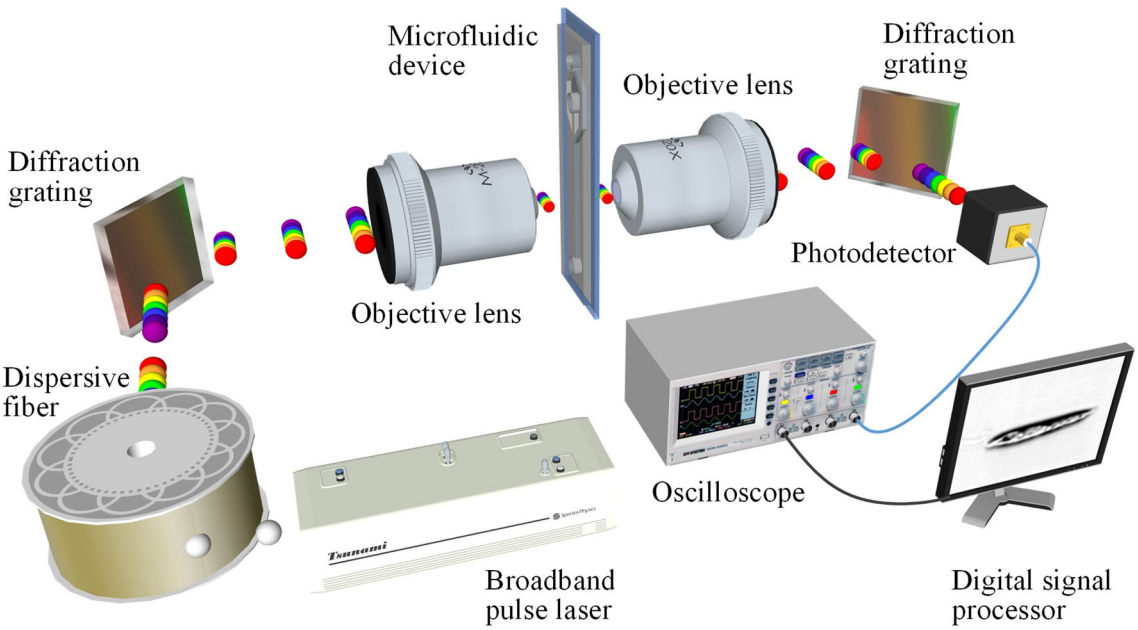

Fig. 1 Schematic of optofluidic time-stretch microscopy. A pulse from the broadband pulse laser is time-stretched by the dispersive fiber. The time-stretched pulse is diffracted by the first diffraction grating into a 1D rainbow pulse, which is incident via the first objective lens onto the target in the microfluidic device. The transmitted rainbow pulse is collected by the second objective lens and recombined by the second diffraction grating into a pulse. The pulse is detected by the photodetector and digitized by the oscilloscope. The pulse is repeated at the pulse repetition rate of the laser. A 2D image of the target is constructed by digitally stacking the 1D pulses in the flow direction

spectrum of the pulse. Next, the encoded pulse is collected and recombined by the other objective lens and the other spatial disperser (diffraction grating). At last, the pulse is detected and digitized by the single-pixel photodetector and the digitizer, respectively. The pulse is repeated at the laser's pulse repetition rate. While the target flows in the direction perpendicular to the rainbow spread, the optical pulses keep coming at the fixed repetition rate, which is limited by the sampling rate of the digitizer to avoid overlap between adjacent pulses. Thus, each pulse takes one cross section of the target. Finally, digitally stacking the pulses constructs a 2D image of the target.

The order of the temporal disperser with respect to the spatial disperser pair plays an important role in performance. In practice, it is possible to change the order of these two elements, depending on the requirements of specific applications [7]. In general, putting the spatial disperser before the temporal disperser offers a shorter exposure time (or a higher shutter speed), which is preferable for imaging of highly dynamic targets or phenomena. On the other hand, placing the temporal disperser before the spatial disperser relieves photodamage to the targets and avoids distortion in the images caused by unwanted nonlinear interactions in the temporal disperser.

As shown in Fig. 1, cell focusing is important in optofluidic time-stretch microscopy as it requires cells to arrive at the same set of spatial coordinates in the optical interrogation region. For this reason, a hydrodynamic focusing microfluidic device [14] is often used to channel and focus the cells. Alternatively, one can also use an inertial focusing microfluidic device [15] or an acoustic focusing microfluidic device [16] to manipulate the flow characteristics of the cells.

2.2 Basic performance of optofluidic time-stretch microscopy

The performance of optofluidic time-stretch microscopy can be evaluated with both static and fast-flowing cells in terms of spatial resolution and image quality, quantitatively as well as qualitatively. As the key process in optofluidic time-stretch microscopy, dispersive Fourier transformation plays a defining role in the performance of the whole system. To verify the reliability of the dispersive Fourier transformation, we show the temporal waveform and spectrum of a time-stretched pulse together in Fig. 2a [9, 17]. It is clear that after the dispersive Fourier transformation, the temporal waveform of the pulse matches its spectrum, which confirms a lossless recovery of the spatial discrimination of the target. The spatial resolution of an optofluidic time-stretch microscope is fundamentally limited by the center wavelength of the optical pulses and the numerical aperture of the objective lens. To quantitatively evaluate the spatial resolution of the optofluidic time-stretch microscope, we used an 800-nm broadband pulse laser and a pair of 0.65-NA objective lenses to construct an optofluidic time-stretch microscope, and employed it to image a standard USAF-1951 resolution chart. To acquire the 2D patterns of this chart, we used a translation stage to align it to the area irradiated by the 1D rainbow pulses. Figure 2b shows an obtained image of the resolution chart, where the line pairs in group 9 are clearly recognizable, indicating that the spatial resolution of the microscope is higher than 780 nm (given that the line width of group 9 element 3 is 780 nm on the resolution chart) [9]. In addition, to show the capability of optofluidic time-stretch microscopy to acquire high-quality images at a high throughput, we used an optofluidic time-stretch microscope and a conventional optical microscope to image the same type of cells in high-speed flow and in stationary state, respectively. Images of the cells, specifically MCF-7 cells (a breast cancer cell line), acquired by these two different methods are shown in Fig. 2c [13]. Although the cells were flowing at a high speed of 10 m/s, phenotypic features of the cells can clearly be recognized in the case of optofluidic time-stretch microscopy while the images are of comparable quality to that of static images obtained with conventional optical microscopy.

3 Applications of optofluidic time-stretch microscopy

Optofluidic time-stretch microscopy's advantages over conventional methods make it applicable to various fields where high-throughput and high-precision single-cell analysis is needed. In this section, we introduce three unique applications of optofluidic time-stretch microscopy that meet the requirements: characterization of microalgal cells for green energy production, detection of aggregated platelets for evaluation of thrombotic disorders, and detection of cellular drug responses for drug screening and discovery.

3.1 Characterization of microalgal cells for green energy production

Due to a limited supply of fossil fuels and the adverse effects of increasing atmospheric CO_2 levels, the development of reliable, sustainable, and economical sources of alternative fuels is globally pursued scientific responsibility [18]. As an alternative to liquid fossil fuels, algal biofuel has attracted much attention from the scientific community over the last decade because it requires minimal environmental resources, recycles atmospheric CO_2, and can be grown even in saline and wastewater. Among various types of algae for biofuel production, *Euglena gracilis*, a species of unicellular flagellate protists found in fresh water, is attractive as it is known to produce wax ester and triacylglycerol within lipid droplets

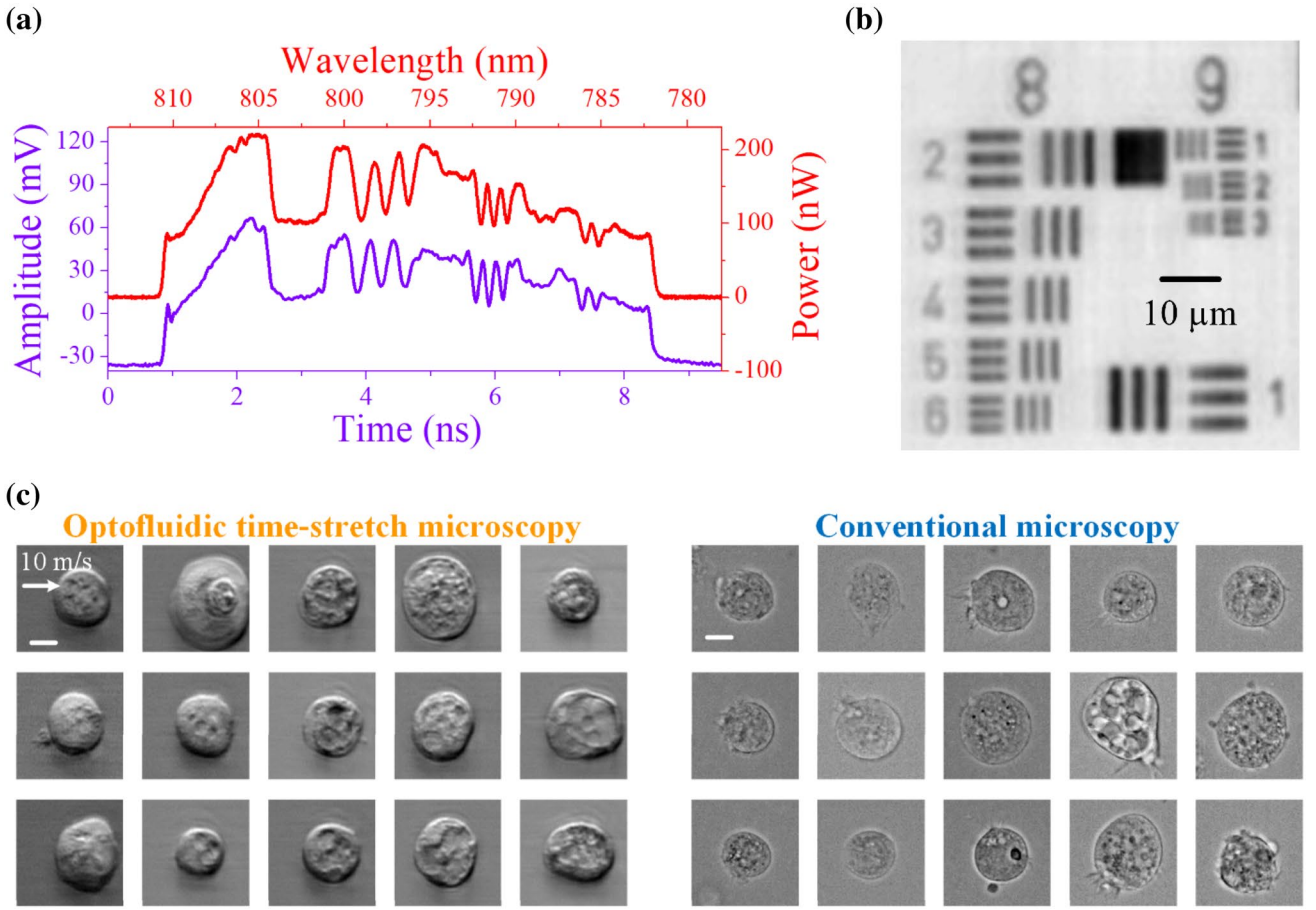

Fig. 2 Basic performance of optofluidic time-stretch microscopy. **a** Temporal waveform and corresponding spectrum of a time-stretched laser pulse. **b** Image of a standard USAF-1951 resolution chart. **c** Images of MCF-7 (breast cancer) cells acquired by optofluidic time-stretch microscopy (in flow) and conventional microscopy (static). Scale bars: 10 µm

(which can be refined to produce kerosene suitable as a jet fuel) [19]. To date, several techniques for lipid induction or genetic engineering have been developed to increase the efficiency of lipid production in microalgae such as *E. gracilis* [20]. Unfortunately, despite the availability of such lipid induction techniques, their effect on heterogeneous microalgal cells has not been fully explored due to the lack of analytical tools and fluorescent probes that allow rapid interference-free or non-invasive evaluation of large numbers of single cells. Compared with conventional methods, optofluidic time-stretch microscopy has proven to be a feasible method to evaluate the outcome of lipid induction in a rapid and non-invasive manner and holds promise for optimizing the efficiency of biofuel production based on *E. gracilis* and potentially other types of microalgae.

To evaluate the performance of characterizing *E. gracilis* cells, we prepared three types of *E. gracilis* cells, namely fresh *E. gracilis* cells, mature *E. gracilis* cells and lipid-accumulated *E. gracilis* cells. The cultures (provided by the Microbial Culture Collection at the National Institute for Environmental Studies, Japan) were grown in flasks with a working volume of 20 mL, each under a 14/10 light/dark illumination cycle (130–150 µmol/m^2/s) at 25 °C. The stock culture of *E. gracilis* was grown in an autotrophic medium, AF-6 [10] as a pre-culture for at least 6 days. To prepare fresh *E. gracilis* cells, we kept the cells in the exponential growth phase in the AF-6 medium. To prepare mature *E. gracilis* cells, we kept the cells in the stationary growth phase in the AF-6 medium. To prepare lipid-accumulated *E. gracilis* cells, the cells were grown in the AF-6–N medium (nitrogen nutrient omitted from AF-6) for 5 days after cultivation.

Image libraries of these three types of *E. gracilis* cells acquired by optofluidic time-stretch microscopy are shown in Fig. 3a. From the images, it is apparent that fresh *E. gracilis* cells look notably more transparent than the other two types. Although mature and lipid-accumulated *E. gracilis* cells look similar with respect to the quantity of scatterers, their local distributions are different. In mature *E. gracilis* cells, the scatterers form several clusters, typically leaving a transparent belt

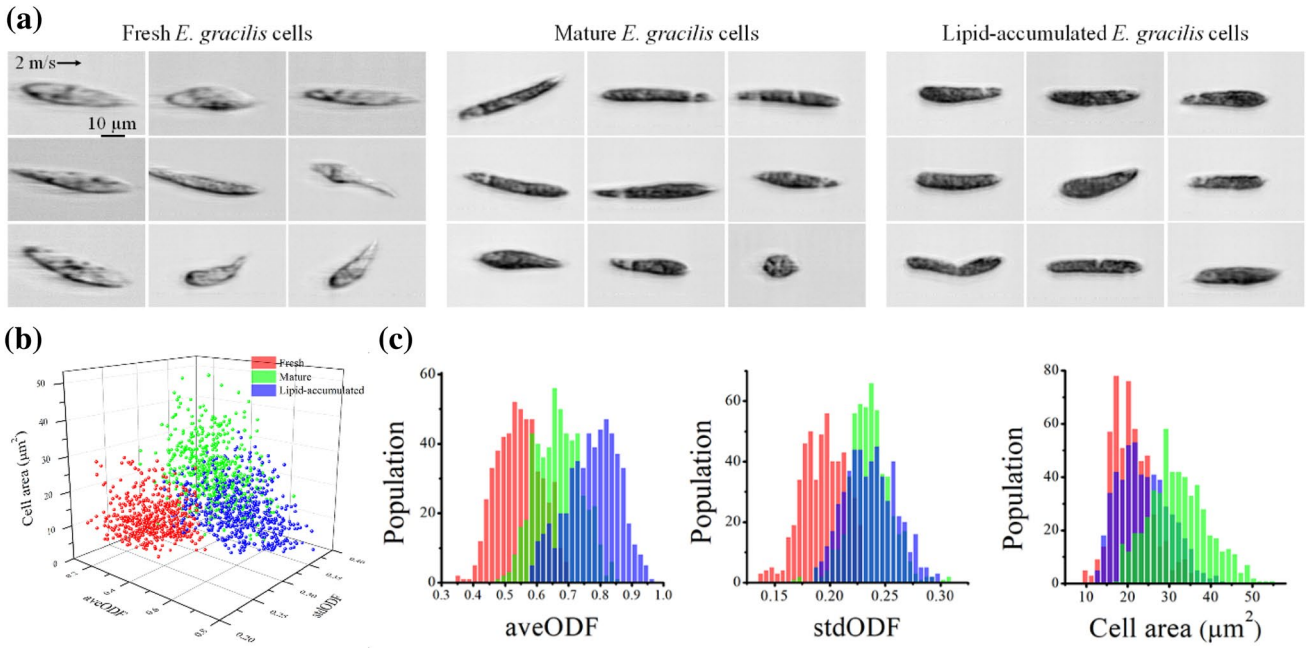

Fig. 3 Optofluidic time-stretch microscopy of *E. gracilis* cells. **a** Images of the cells under different culture conditions. **b** 3D scatter plot of the cells correlating cellular area, average value of the ODF, and standard deviation of the ODF. **c** 1D histograms of cellular area, average value of the ODF, and standard deviation of the ODF

in the middle of the cell. In contrast, such scatterers tend to occupy the whole body in the lipid-accumulated cells, turning it almost completely opaque. We used the opacity distribution function (ODF) [10] to quantitatively analyze these images. Specifically, after segmenting the cell images, we calculated cell area and ODF for every image. To visualize the differences between these three types of cells, we plotted all cellular images as single points in a 3D space which was spanned by cell area, average value of the ODF, and standard deviation of the ODF (Fig. 3b). Here, different colors represent different cell types. Fresh *E. gracilis* cells are indicated in red, mature *E. gracilis* cells in green, and lipid-accumulated *E. gracilis* cells in blue. In addition, we separately show three 1D histograms of each cell in Fig. 3c. From the 3D scatter plot, it is clear that those three types of *E. gracilis* cells can indeed be distinguished by the optofluidic time-stretch microscope. More specific information can be obtained from the three 1D histograms: the histogram in stdODF indicates that cell-to-cell variations become larger as the amount of nitrogen in the culture medium decreases. The cellular histograms constructed with respect to cell area shows that the overall area of mature cells is the largest among these three types of *E. gracilis* cells.

3.2 Detection of aggregated platelets for evaluation of thrombotic disorders

According to WHO, about 10 million new cases of thrombotic disorders are diagnosed worldwide every year [21], leading to a lethality rate that is higher than that of AIDS, prostate cancer, breast cancer, and traffic accidents combined in the US and Europe [22]. There exists scientific evidence that the presence of aggregated platelets in the blood stream caused by platelet activation is involved in thrombotic disorders, especially acute myocardial infarction, and thus may serve as a potential biomarker for the disease [23, 24]. However, conventional methods such as Coulter counting and fluorescence-activated cell sorting (FACS) fail to effectively detect aggregated platelets in blood. This is, on the one hand, caused by a lack of spatial discrimination (Coulter counter), making cells indistinguishable from cell clusters with similar sizes [25], and, on the other hand, due to the dependence on fluorescence labeling (FACS), which can cause unexpected platelet aggregation and result in incorrect counts. Furthermore, the efficiency of imaging flow cytometry methods, despite the excellent accuracy achieved in detection, remains highly limited by the low image acquisition rate (< 1000 frames per second) of currently available commercial imaging sensors such as CCD and CMOS image sensors [26]. In this context, optofluidic time-stretch microscopy can be an ideal tool to visually detect aggregated platelets in blood in a label-free manner for evaluation and monitoring of thrombotic disorders.

Our protocol for the proof-of-principle detection of platelet aggregates is as follows. We obtained blood samples from several healthy donors, using vacuum tubes with sodium citrate that were then processed for measurements.

Since we mainly focused on the platelets in blood, we lysed red blood cells in the samples. We used collagen to induce platelet aggregation prior to the measurements. To provide a ground truth for all optofluidic time-stretch microscopy measurements, we labeled the samples with anti-CD61-APC antibodies (IOTest) and anti-CD62P-PE antibodies (BD Biosciences). Here CD61-APC was expressed on all platelets whereas CD62P-PE was expressed only on activated or aggregated platelets. To obtain the morphological images and fluorescence signals of the blood cells simultaneously, we employed an optofluidic time-stretch microscope with a fluorescence detector [9, 27]. The samples were diluted with normal saline to maintain a cell concentration around 10^7 cells/mL. All the samples were measured within 5 h after preparation at room temperature (about 25 °C). This study was approved by the Research Ethics Committee at the University of Tokyo. All experiments were performed in accordance with relevant guidelines and regulations. A written informed consent was obtained from all blood donors.

The measurement results are shown in Fig. 4. Since only red blood cells were lysed prior to the measurements, the three main cell types obtained were single platelets, aggregated platelets, and white blood cells whose images and corresponding fluorescence signals are shown in Fig. 4a. Owing to their minute size, it is clear that for single platelets only the fluorescence signals of CD61-APC can be detected. The aggregated platelets look much larger and granular while fluorescence signals of both CD61-APC and CD62P-PE can be detected. Unlabeled white blood cells look spherical and do not give rise to a fluorescence signal. The good agreement between acquired images and their respective fluorescence signals (Fig. 4a) suggests that it is possible to identify and

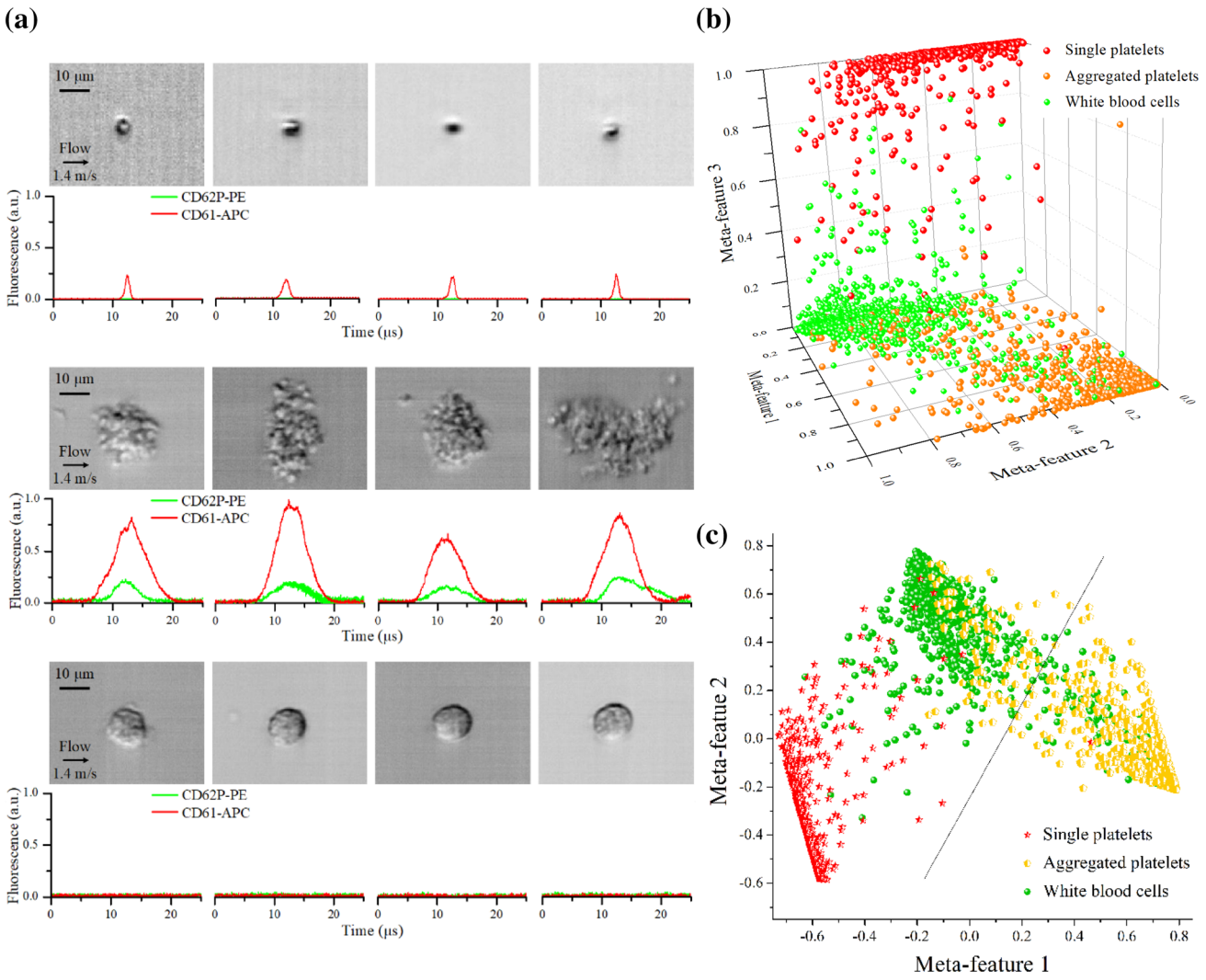

Fig. 4 Optofluidic time-stretch microscopy of blood cells. **a** Images and fluorescence signals of single platelets, aggregated platelets, and white blood cells. **b** 3D scatter plot of single platelets, aggregated platelets, and white blood cells in terms of three meta-features. **c** 2D projection of the 3D scatter plot to maximize the separation between the cell groups for the identification of aggregated platelets

distinguish these three types of blood cells via their morphological features. Therefore, we used fluorescence signals as a reliable ground truth, and performed image-based cell classification with a standard logistic regression model. The three types of cells, shown in different colors, are plotted in a 3D scatter plot in Fig. 4b. The three axes of the scatter plot represent three meta-features, meaning that they are linear combinations of all morphological features of the cells. The 2D projection of the 3D scatter plot in Fig. 4b to maximize the separation between the cell groups is shown in Fig. 4c. The specificity and sensitivity of platelet-aggregation detection was calculated to be 96.6 and 96.6%, respectively. It is clear that the technique can effectively distinguish these three types of cells based on their morphological features in a label-free manner, which is not possible in conventional non-imaging flow cytometry [12].

3.3 Detection of cellular drug responses

Research shows that drug-induced phenotypic variations of cells in gene expression, protein localization, and cytoskeletal structure can be used to predict cellular drug responses and are, hence, important for drug discovery [28]. High-content analysis as opposed to conventional univariate analysis methods is considered as a superior tool for evaluating such variations because of its capability to acquire cellular images from which large numbers of treatment-related variables can be extracted [4, 29]. However, the requirement for fluorescent labeling intrinsically limits the feasibility of high-content analysis in drug discovery for several reasons. First, since fluorescent probes are not available for all target molecules, it is not applicable for the investigation of targets for which fluorescent probes are unavailable. Second, fluorescent labeling's invasive nature may interfere with natural cellular functions which can lead to incorrect results [30]. Finally, fluorescent labeling is costly and time consuming, usually requiring additional processing and compromising cell viability [31]. Therefore, high-content analysis without the need for fluorescent labeling is highly demanded for cellular drug response detection. Considered for its excellent performance in image-based high-throughput and high-accuracy single-cell analysis, optofluidic time-stretch microscopy ranks among the most capable candidates for this application.

To demonstrate the effectiveness of optofluidic time-stretch microscopy in cellular drug response detection, we used MCF-7 (DS Pharma Biomedical), a human breast adenocarcinoma cell line, and paclitaxel (Cayman Chemical), an FDA-approved anti-cancer drug, as the model cell and drug, respectively. Before measurement, the MCF-7 cells were maintained in Dulbecco's modified Eagle medium (DMEM) (Wako Chemicals) supplemented with 10% fetal bovine serum (MP Biomedicals) and 1% penicillin–streptomycin (Wako Chemicals), at 37 °C and 5% CO_2. The powder-form paclitaxel was dissolved in dimethyl sulfoxide (DMSO, Wako Chemicals) to a stock concentration of 1 mM. 24 h after seeding, the MCF-7 cells were divided into six groups, which were incubated with dilutions of paclitaxel with different concentrations (0 nM/negative control, 1, 10, 100 nM, 1 and 10 μM). After 24-h treatment, the cells were suspended in the culture medium by trypsinization, and processed to cellular solution with a concentration around 10^5–10^6 cells/mL for subsequent measurements by optofluidic time-stretch microscopy.

Measurement results and their analysis are shown in Fig. 5. To highlight the capability of optofluidic time-stretch microscopy in obtaining high-quality cellular images at a high flow rate, we show the images of drug-treated and -untreated MCF-7 cells captured by both the optofluidic time-stretch microscope and a conventional optical microscope in Fig. 5a. Although the MCF-7 cells were flowing at a speed as high as 10 m/s, the cellular images acquired with the optofluidic time-stretch microscope clearly show the phenotypes of cells with high contrast and a quality comparable with what a conventional optical microscope can achieve. To quantitatively evaluate morphological changes of MCF-7 cells after treatment with paclitaxel, we performed support vector machine (SVM)-based classification between the negative control and the cells treated with different concentrations of paclitaxel based on 548 morphological features extracted from each cellular image. The classification accuracy at various concentrations is shown in Fig. 5b. From this curve, a dose dependence of drug-induced morphological changes can clearly be observed. Moreover, we used the maximum mean discrepancy (MMD) [13] to evaluate the contributions of these 548 features to the classification. MMD is routinely used to measure the distance between two high-dimensional distributions. Consequently, a feature with high MMD score indicates a strong contribution and thus a high importance for the classification. We calculated the MMD scores for each feature and performed SVM classification using features with large MMD scores. As Fig. 5c shows, as the number of features used in the classification decreases, the classification accuracy also decreases. However, a classification accuracy over 90% can be maintained as long as more than 100 features are used in the classification.

4 Summary

In summary, optofluidic time-stretch microscopy is an ideal tool for high-throughput and high-precision flow cytometry of single cells in large heterogeneous populations. By virtue of its ability to generate numerous bright-field cell images, it provides the level of specificity comparable to fluorescence imaging. In this paper, we have discussed the principles and

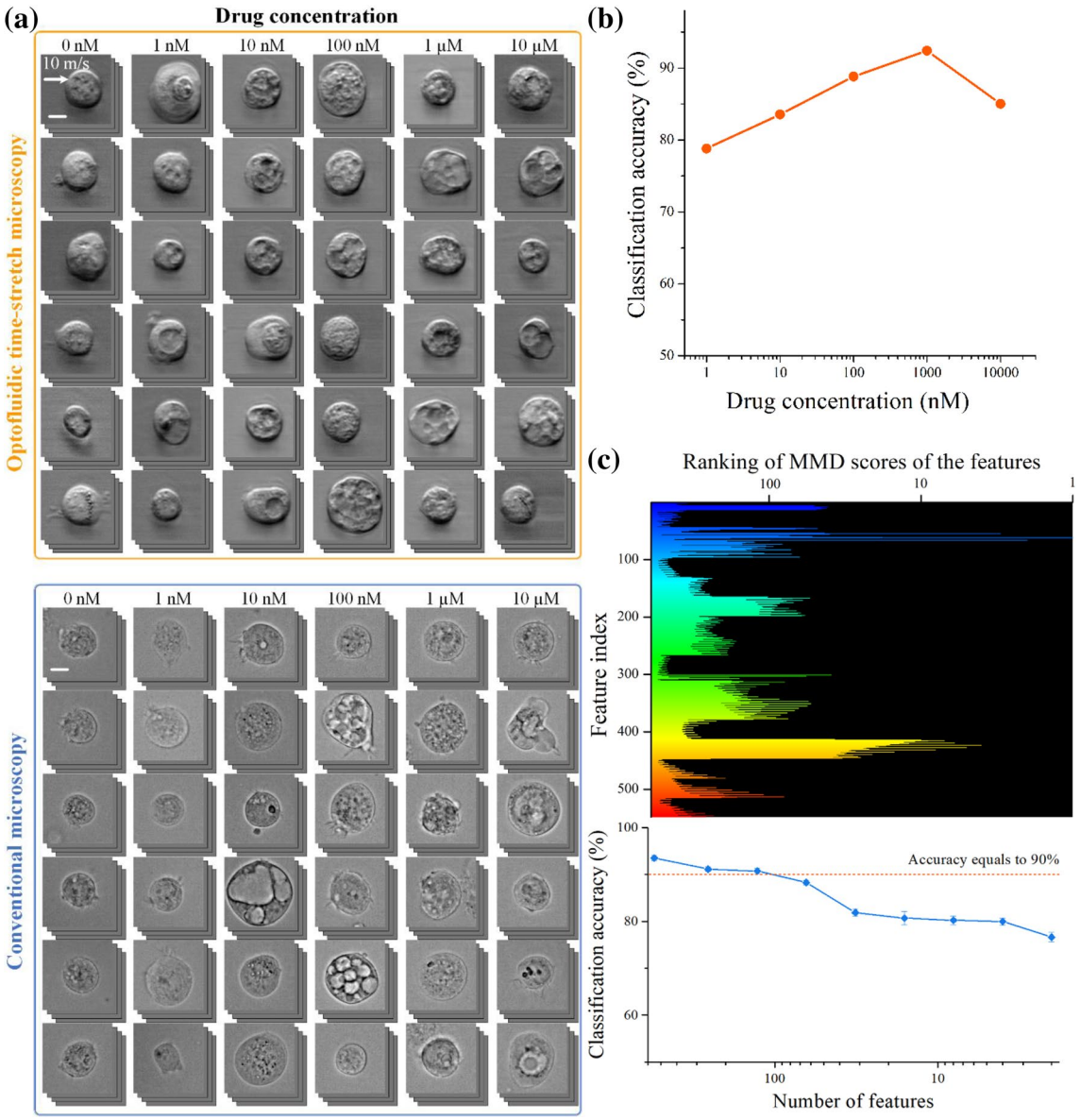

Fig. 5 Optofluidic time-stretch microscopy of MCF-7 (breast cancer) cells. **a** Image libraries of MCF-7 cells treated with different concentrations of drugs acquired by optofluidic time-stretch microscopy and conventional microscopy. **b** Classification accuracy between negative control and cells treated with various concentrations of drugs. **c** Classification accuracy with different numbers of features. Scale bars: 10 μm

configuration of an optofluidic time-stretch microscope and its applications in three important fields where the method is found useful. It is our hope that this review paper serves as a guidebook that helps readers apply this method to their research and development in diverse biomedical science.

Acknowledgements This work was primarily funded by the ImPACT Program of the CSTI (Cabinet Office, Government of Japan) and partly by Noguchi Shitagau Research Grant, New Technology Development Foundation, Konica Minolta Imaging Science Encouragement Award, JSPS KAKENHI Grant numbers 25702024 and 25560190, JGC-S Scholarship Foundation, Mitsubishi Foundation, TOBIRA Award, and Takeda Science Foundation. K. G. was partly supported by Burroughs Wellcome Foundation. The fabrication of the microfluidic device was conducted at the Center for Nano Lithography & Analysis, University of Tokyo, supported by the MEXT, Japan.

Compliance with ethical standards

Conflict of interest The authors declare no competing financial interests.

References

1. Goda, K., Ayazi, A., Gossett, D.R., Sadasivam, J., Lonappan, C.K., Sollier, E., Fard, A.M., Hur, S.C., Adam, J., Murray, C., Wang, C., Brackbill, N., Di Carlo, D., Jalali, B.: High-throughput single-microparticle imaging flow analyzer. Proc. Natl. Acad. Sci. **109**(29), 11630–11635 (2012)
2. Malo, N., Hanley, J.A., Cerquozzi, S., Pelletier, J., Nadon, R.: Statistical practice in high-throughput screening data analysis. Nat. Biotechnol. **24**(2), 167–175 (2006)
3. Corash, L.: Measurement of platelet activation by fluorescence-activated flow cytometry. Blood Cells **16**(1), 97–108 (1990)
4. Usaj, M.M., Styles, E.B., Verster, A.J., Friesen, H., Boone, C., Andrews, B.J.: High-content screening for quantitative cell biology. Trends Cell Biol. **26**(8), 598–611 (2016)
5. Porichis, F., Hart, M.G., Griesbeck, M., Everett, H.L., Hassan, M., Baxter, A.E., Lindqvist, M., Miller, S.M., Soghoian, D.Z., Kavanagh, D.G., Reynolds, S., Norris, B., Mordecai, S.K., Quan, N., Lai, C., Kaufmann, D.E.: High-throughput detection of miRNAs and gene-specific mRNA at the single-cell level by flow cytometry. Nat. Commun. **5**, 5641 (2014)
6. Goda, K., Tsia, K.K., Jalali, B.: Serial time-encoded amplified imaging for real-time observation of fast dynamic phenomena. Nature **458**(7242), 1145–1149 (2009)
7. Lei, C., Guo, B., Cheng, Z., Goda, K.: Optical time-stretch imaging: principles and applications. Appl. Phys. Rev. **3**(1), 011102 (2016)
8. Lau, A.K., Shum, H.C., Wong, K.K., Tsia, K.K.: Optofluidic time-stretch imaging—an emerging tool for high-throughput imaging flow cytometry. Lab Chip **16**(10), 1743–1756 (2016)
9. Ugawa, M., Lei, C., Nozawa, T., Ideguchi, T., Di Carlo, D., Ota, S., Ozeki, Y., Goda, K.: High-throughput optofluidic particle profiling with morphological and chemical specificity. Opt. Lett. **40**(20), 4803–4806 (2015)
10. Lei, C., Ito, T., Ugawa, M., Nozawa, T., Iwata, O., Maki, M., Okada, G., Kobayashi, H., Sun, X., Tiamsak, P., Tsumura, N., Suzuki, K., Di Carlo, D., Ozeki, Y., Goda, K.: High-throughput label-free image cytometry and image-based classification of live *Euglena gracilis*. Biomed. Opt. Express **7**(7), 2703–2708 (2016)
11. Lai, Q.T.K., Lee, K.C.M., Tang, A.H.L., Wong, K.K.Y., So, H.K.H., Tsia, K.K.: High-throughput time-stretch imaging flow cytometry for multi-class classification of phytoplankton. Opt. Express **24**(25), 28170–28184 (2016)
12. Jiang, Y., Lei, C., Yasumoto, A., Kobayashi, H., Aisaka, Y., Ito, T., Guo, B., Nitta, N., Kutsuna, N., Ozeki, Y., Nakagawa, A., Yatomi, Y., Goda, K.: Label-free detection of aggregated platelets in blood by machine-learning-aided optofluidic time-stretch microscopy. Lab Chip **17**(14), 2337–2530 (2017)
13. Kobayashi, H., Lei, C., Wu, Y., Mao, A., Jiang, Y., Guo, B., Ozeki, Y., Goda, K.: Label-free detection of cellular drug responses by high-throughput bright-field imaging and machine learning. Sci. Rep. **7**(1), 12454 (2017)
14. Golden, J.P., Justin, G.A., Nasir, M., Ligler, F.S.: Hydrodynamic focusing-a versatile tool. Anal. Bioanal. Chem. **402**(1), 325–335 (2012)
15. Di Carlo, D.: Inertial microfluidics. Lab Chip **9**(21), 3038–3046 (2009)
16. Grenvall, C., Antfolk, C., Bisgaard, C.Z., Laurell, T.: Two-dimensional acoustic particle focusing enables sheathless chip Coulter counter with planar electrode configuration. Lab Chip **14**(24), 4629–4637 (2014)
17. Goda, K., Jalali, B.: Dispersive Fourier transformation for fast continuous single-shot measurements. Nat. Photonics **7**(2), 102–112 (2013)
18. Fargione, J., Hill, J., Tilman, D., Polasky, S., Hawthorne, P.: Land clearing and the biofuel carbon debt. Science **319**(5867), 1235–1238 (2008)
19. Giometto, A., Altermatt, F., Maritan, A., Stocker, R., Rinaldo, A.: Generalized receptor law governs phototaxis in the phytoplankton *Euglena gracilis*. Proc. Natl. Acad. Sci. **112**(22), 7045–7050 (2015)
20. Rezic, T., Filipovic, J., Santek, B.: Photo-mixotrophic cultivation of algae *Euglena gracilis* for lipid production. Agric. Conspec. Sci. **78**(1), 65–69 (2013)
21. Wilson, R.M., Michel, P., Olsen, S., Gibberd, R.W., Vincent, C., El-Assady, R., Rasslan, O., Qsous, S., Macharia, W.M., Sahel, A., Whittaker, S., Abdo-Ali, M., Letaief, M., Ahmed, N.A., Abdellatif, A., Larizgoitia, I., Worki, W.H.: O.P.S.E.A.: patient safety in developing countries: retrospective estimation of scale and nature of harm to patients in hospital. Br. Med. J. **344**, e832 (2012)
22. Raskob, G.E., Angchaisuksiri, P., Blanco, A.N., Buller, H., Gallus, A., Hunt, B.J., Hylek, E.M., Kakkar, A., Konstantinides, S.V., McCumber, M., Ozaki, Y., Wendelboe, A., Weitz, J.I., World, I.S.C.: Thrombosis: a major contributor to the global disease burden. J. Thromb. Haemost. **12**(10), 1580–1590 (2014)
23. Jackson, S.P.: The growing complexity of platelet aggregation. Blood **109**(12), 5087–5095 (2007)
24. Fabre, J.E., Nguyen, M.T., Latour, A., Keifer, J.A., Audoly, L.P., Coffman, T.M., Koller, B.H.: Decreased platelet aggregation, increased bleeding time and resistance to thromboembolism in $P2Y_1$-deficient mice. Nat. Med. **5**(10), 1199–1202 (1999)
25. Bull, B.S., Schneiderman, M.A., Brecher, G.: Platelet counts with the Coulter counter. Am. J. Clin. Pathol. **44**(6), 678–688 (1965)
26. Satoh, K., Yatomi, Y., Kubota, F., Ozaki, Y.: Small aggregates of platelets can be detected sensitively by a flow cytometer equipped with an imaging device: mechanisms of epinephrine-induced aggregation and antiplatelet effects of beraprost. Cytometry **48**(4), 194–201 (2002)
27. Guo, B., Lei, C., Ito, T., Jiang, Y., Ozeki, Y., Goda, K.: High-throughput accurate single-cell screening of *Euglena gracilis* with fluorescence-assisted optofluidic time-stretch microscopy. PLoS One **11**(11), e0166214 (2016)
28. Futamura, Y., Kawatani, M., Kazami, S., Tanaka, K., Muroi, M., Shimizu, T., Tomita, K., Watanabe, N., Osada, H.: Morphobase, an encyclopedic cell morphology database, and its use for drug target identification. Chem Biol **19**(12), 1620–1630 (2012)
29. Heynen-Genel, S., Pache, L., Chanda, S.K., Rosen, J.: Functional genomic and high-content screening for target discovery and deconvolution. Expert Opin. Drug Dis. **7**(10), 955–968 (2012)
30. Wojcik, K., Dobrucki, J.W.: Interaction of a DNA intercalator DRAQ5, and a minor groove binder SYTO17, with chromatin in live cells-influence on chromatin organization and histone-DNA interactions. Cytom. A **73A**(6), 555–562 (2008)
31. Blasi, T., Hennig, H., Summers, H.D., Theis, F.J., Cerveira, J., Patterson, J.O., Davies, D., Filby, A., Carpenter, A.E., Rees, P.: Label-free cell cycle analysis for high-throughput imaging flow cytometry. Nat. Commun. **7**, 10256 (2016)